Supplementary Information

Electro-catalytic degradation pathway and mechanism of acetamiprid using Er doped Ti/SnO_2–Sb electrode

Shanping Li[a, b,*], Yahui Li[a], Xueyuan Zeng[a], Wenran Wang[a], Ruoxin Shi[a], Lina Ma[a]

a. School of Environmental Science and Engineering, Shandong University, 27 Shandananlu, Jinan, 250100, China.

b. Shandong Key Laboratory of Water Pollution Control and Resource Reuse, Jinan, 250100, China

E-mail: lishanping@sdu.edu.cn

Corresponding author. Professor Shanping Li Tel.:+86 0531-88362872; fax: +86 0531-88362872

1. Structural characterization of the electrode

The morphologies of the anode before and after 5h electrolysis run were done with a Japanese JEOL company model JSM-7600F microscope, equipped with an energy dispersive spectrometer. The structural analysis was confirmed by a D/max-rA XRD instrument (Rigaku, Japan, Cu Kα, 40kV, 50 mA). The FT-IR analysis of the precursor powder was carried out with a VERTEX-70 FT-IR using the KBr pellet technique. The optical absorption property was measured by using ultraviolet visible diffuse reflectance spectroscopy (UV-Vis DRS, UV-2550, Shimadu) at room temperature in the wavelength region between 220 and 800 nm. Ultrafine $BaSO_4$ powder supplied by Shimadzu Company was used as a reference.

2. SEM and EDS analysis

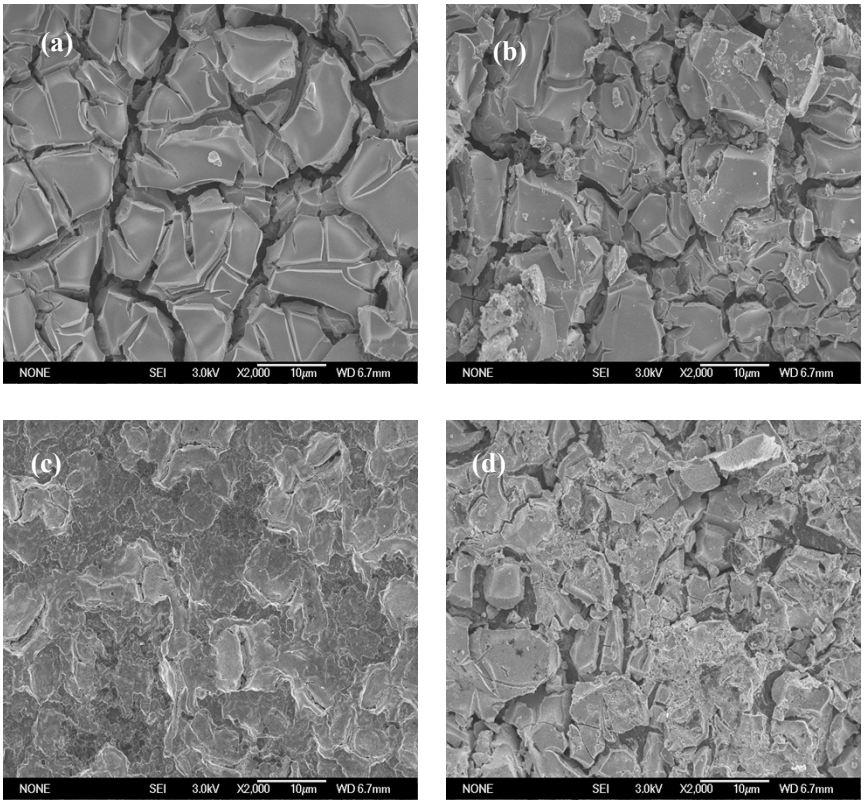

Fig. S1 Representative SEM images of (a) freshly prepared 0 mol% Er-doped, (b) freshly prepared 0.5 mol% Er-doped, (c) 0 mol% Er-doped after 5h electrolysis run and (d) 0.5 mol% Er-doped after 5h electrolysis run Ti/SnO_2-Sb electrode.

The EDS dates of freshly prepared electrodes (Table S1) show that Er doping can promote the surface enrichment of Sb and Er. It was reported that Sb and SnO_2 crystallites may play the role of active sites and was beneficial to the adsorption of polar species[1]. Thus ,the Sb enrichment due to Er addition could be one of the reasons for improving the electro-catalytic ability. The difference between the morphologies of the above mentioned electrodes after 5 h ACT electrolysis(Fig.S1(c) and (d)) also provided an evidence for this view. It was observed that the modified electrode presented a more rough structure with more attachments and smaller coating loss.

Table S1 Composition of elements on two freshly prepared electrodes surfaces

Electrode	Sn	Sb / atomic (%)		Er / atomic (%)	
		Theoretical	Observed	Theoretical	Observed
0 mol% Er doped	100	6	3.45	0	0
0.5 mol% Er doped	100	6	7.81	0.5	3

3. XRD analysis

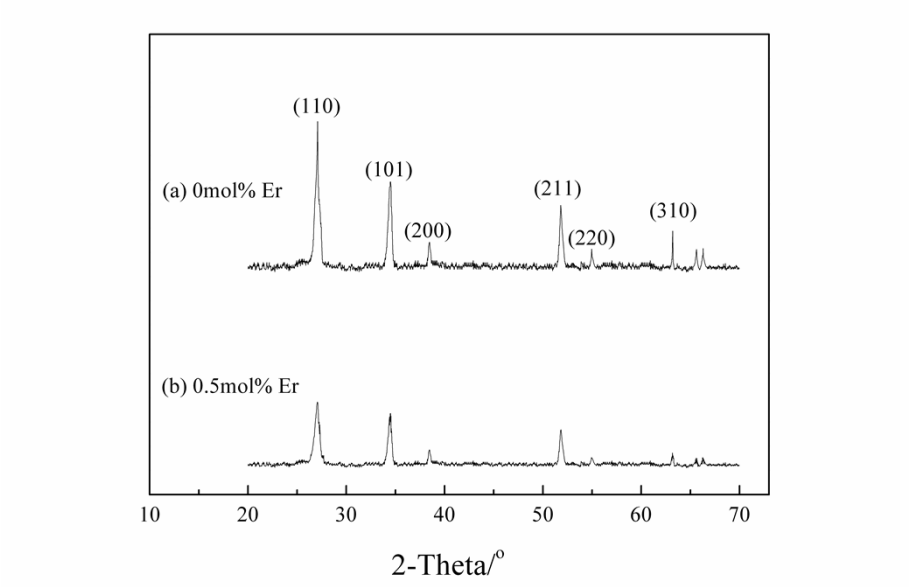

Fig. S2 XRD patterns of freshly prepared electrodes.

Fig. S2 display XRD patterns of the doped and undoped electrodes. The peaks yields of Sn (110,101, 200, 211, 220, 310) are corresponded respectively to the values of 2-Theta (26.6, 34.1, 38.3, 52.0, 54.8, 63.2), which are in line with the tetragonal rutile-type structure of SnO_2 crystallites basically (JCPDS, PDF code: 21-1250). Therefore, the main diffraction peaks confirm the tetragonal rutile-type structure of SnO_2 crystallites. However, the intensity of peaks decreased from Fig. 2(a) to (b).That means that 0.5 mol% Er doped Ti/SnO_2-Sb electrode has smaller grain sizes than 0 mol% Er doped Ti/SnO_2-Sb electrode, which could also be seen from Fig. S1. The result may be explained by the surface segregation of Er as EDS indicates, which may cause the surface composition supercooling to lead the grain refinement[2]. To solid catalysts, a smaller grain size is associated with more surface area and active sites. Therefore, the reduction of grain size also is helpful for the electro-catalytic reaction.

4. FT-IR analysis

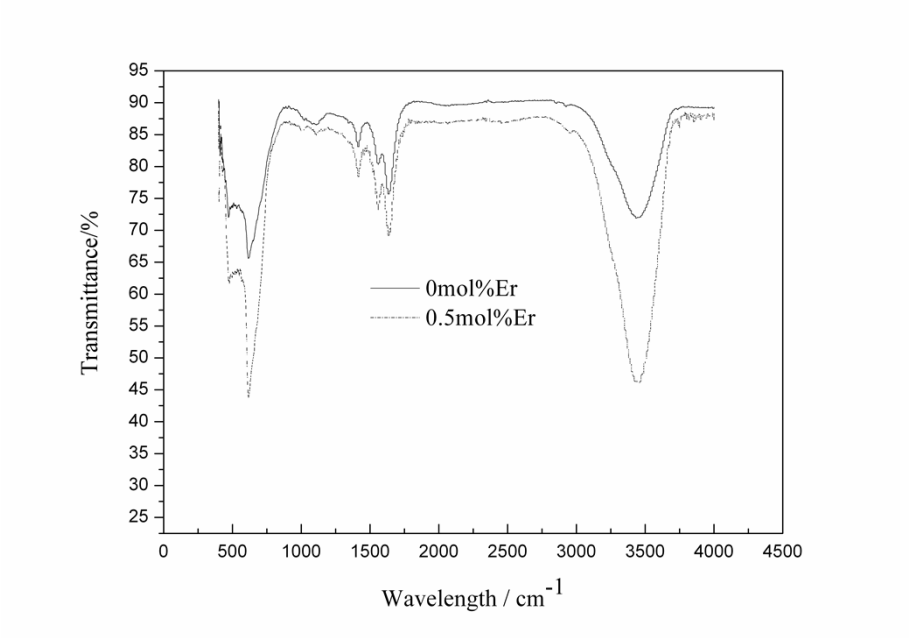

Fig. S3 FT-IR spectra obtained from the precursor solution used for the electrodes preparation with/without Er.

The FT-IR absorption spectra of the precursor powder, prepared by the thermal decomposition of precursor solution with/without Er at 650 ℃, is shown in Fig. S3. The spectra curves observed for two samples were similar in the peak position. The bands at 3430 cm^{-1} could be ascribed to the chemical absorbing water (OH-stretching). The small peak at 1642 cm^{-1} was due to the existing of H_2O in the precipitated phase [3]. The presence of small peaks at 1555 and 1405 cm^{-1} resulted from the formation of COO^- during the calcinations process [3, 4]. The Sn-O stretching vibration of E_u symmetric mode and O-Sn-O variable-angle vibration of A_{2u} symmetric mode could be observed at 617 and 480 cm^{-1}, respectively [5]. No characteristic peak for the doped Er and Sb oxides occurred. This is consistent with XRD analysis. Additionally, it could be seen that there was an obvious increase in the OH-stretching peak at 3430 cm^{-1} from no Er sample to Er modified sample, in comparison to the small change of peak intensity at 1642 cm^{-1}. It seems that Er doping can raise the water absorption of the SnO_2-Sb powder. The behavior would be helpful for the anode surface to product MO_x(•OH).

$$MO_x + H_2O \rightarrow MO_x(HO\cdot) + H^+ + e^- \quad (1)$$

Where MO_x stands for the metal oxides on the anode surface. The peak intensities for Sn-O and O-Sn-O also had significant increase after Er doping. It

suggests that Er promotes the formation of the SnO_2 crystallites. Considering the above mentioned grain refinement, this promotion may mainly accelerate the generation rate, but restrain the growth rate.

5. pH changes analysis

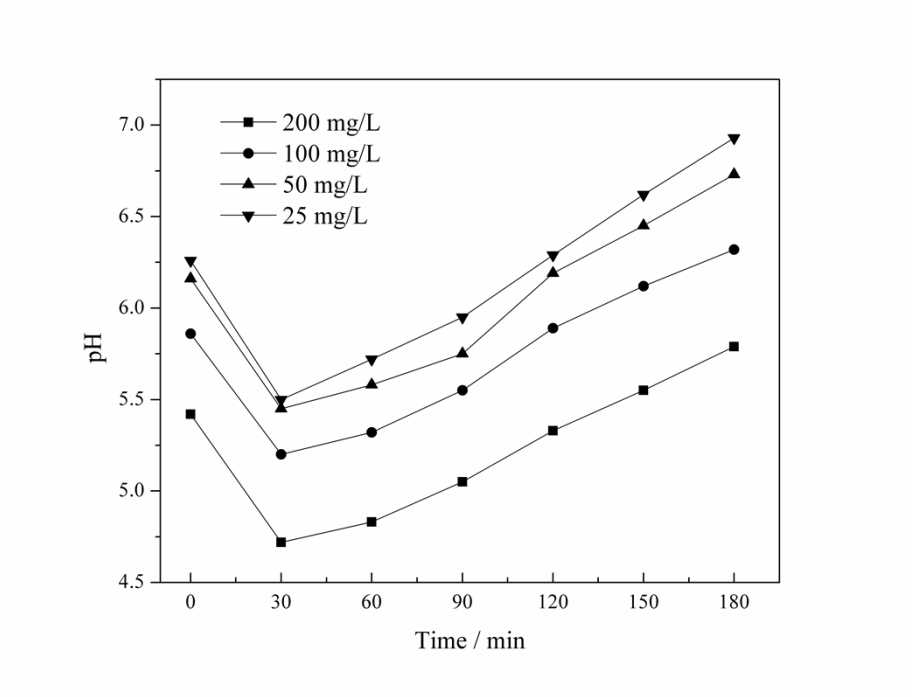

Fig. S4 pH changes at different electrolysis times.

The pH of ATC in electrochemical oxidation process was measured for every 30 minutes. The trend of measured pH with electrolysis time was shown in Fig. S4. The pH of samples decreased from 0 min to 30 min and then increased from 30 to 180 min. As presented in Fig. S4, the solution was always acidic, which indicated the feasibility of Eq. 5-Eq. 8. The increasing of pH from 30 min to 180 min may be due to the transformation of H^+ into H_2 at the cathode possibly.

6. The presence of hydroxyl radicals and hydrogen peroxide

Previous studies [6, 7] showed that n-butanol, which can easily react with •OH (the reaction rate constant was larger than 10^8L/mol•s), could be the scavengers of •OH to reduce the degradation efficiency of organics. The ACT degradation efficiency was measured with the addition of n-butanol in the electrolysis cells. For EC experiments, ACT (50 mg L^{-1}) and n-butanol (50 mg L^{-1}, 100 mg L^{-1}) were placed in cells (140mL) with electrolyte (Na_2SO_4, 0.5 M), respectively, absorbance of the solution was measured to calculate the removal rates shown in Fig. S6.

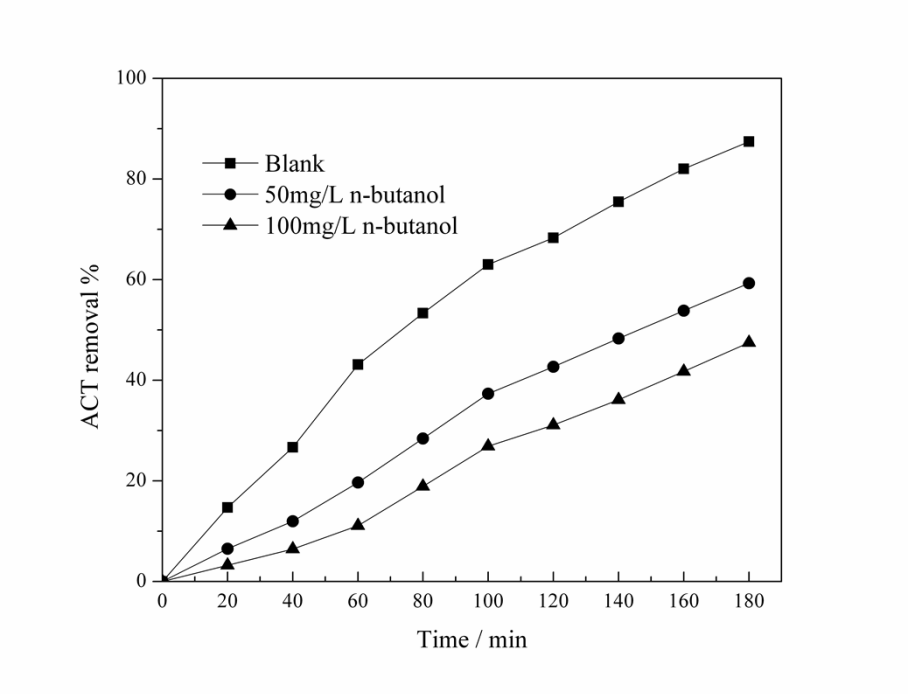

Fig. S6 The effect of adding n-butanol on ACT degradation efficiency.

The addition of n-butanol had a strong inhibition effect of ACT degradation. The higher of n-butanol concentration led to stronger inhibitory effect. When the concentrations of n-butanol were 0 mg/L, 50 mg/L, 100 mg/L, ACT removal efficiencies were 87.45%, 59.21%, 47.46% after 180min, respectively. This observation indicated the presence of hydroxyl radicals played an important role in the degradation process.

The peroxide concentrations were measured by adding with a $TiOSO_4 \cdot xH_2SO_4 \cdot xH_2O$/sulfuric acid solution in the electrolysis cell (pH=3, 5, 7, respectively) [8]. This reagent reacted with hydrogen peroxide quantitatively to form an orange complex whose absorbance was measured at 410 nm after 10min (typically 1.0 ml, diluting to 10 ml). The hydrogen peroxide concentrations were retrieved from the curve of calibrating absorbency value vs. concentration of H_2O_2, as shown in Fig. S7, and the hydrogen peroxide concentrations were shown in Fig. S8, suggesting the presence of H_2O_2.

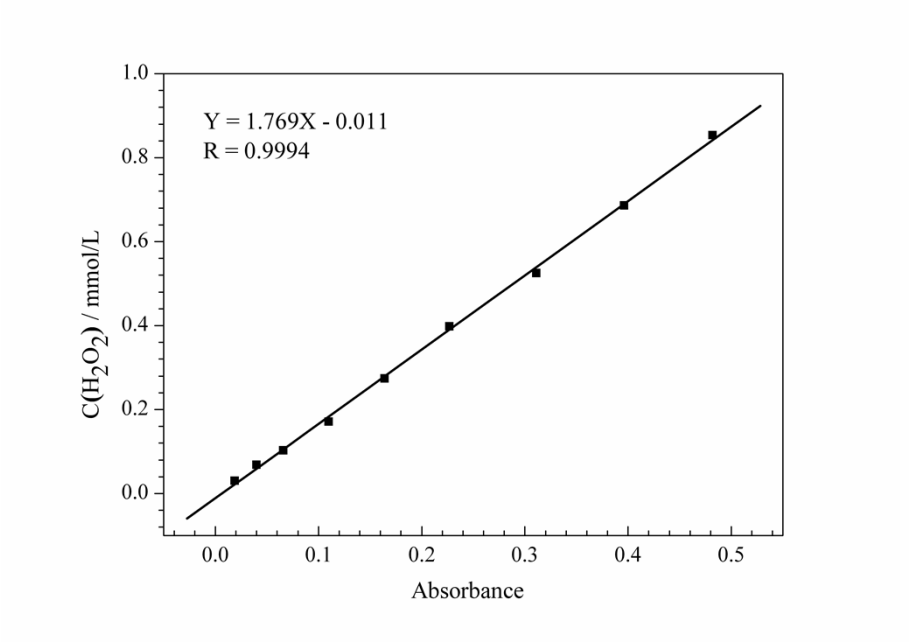

Fig. S7 Calibration of absorbency value vs. concentration of H_2O_2.

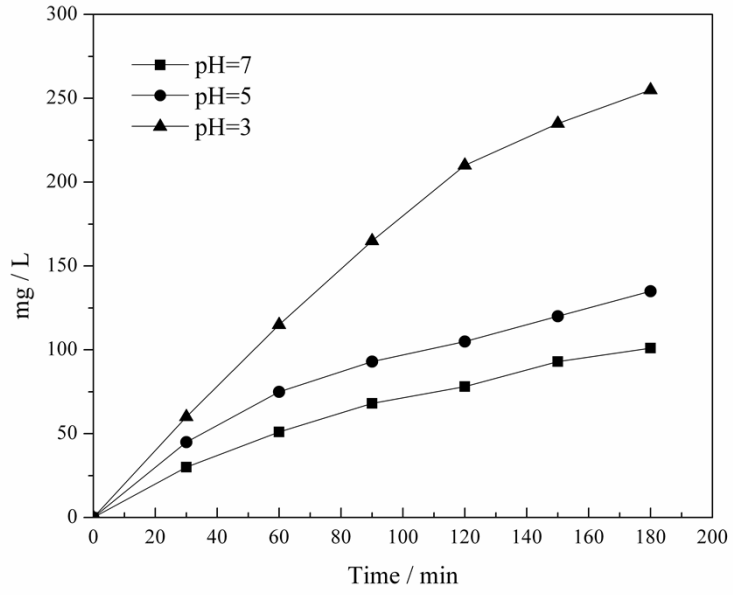

Fig. S8 The concentrations of H_2O_2 at different pH.

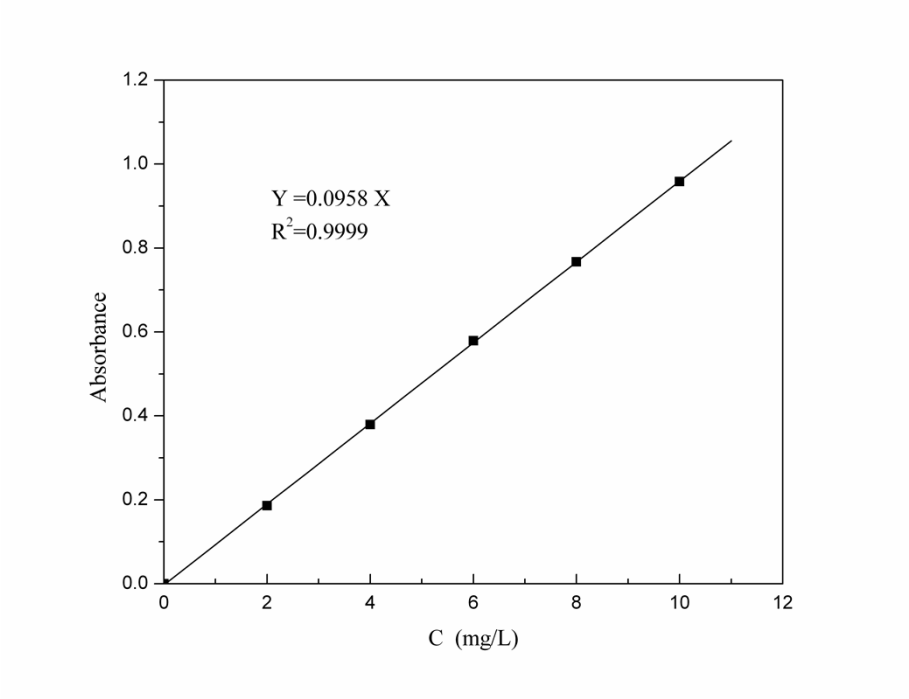

Fig. S5 Calibration of absorbency value vs. concentration of ACT.

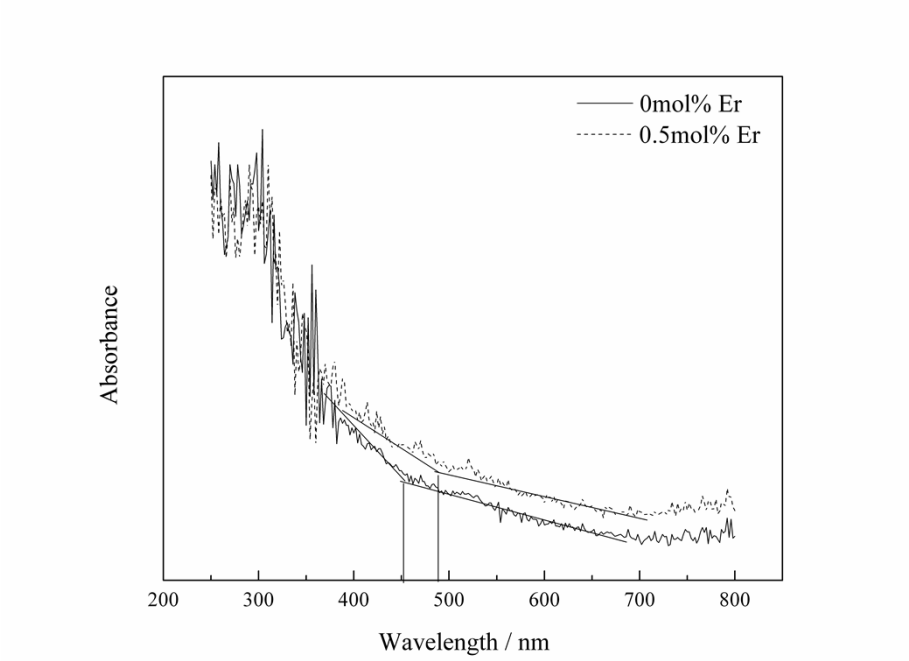

Fig. S9 UV-vis DRS spectra obtained from the precursor powders with or without Er that were used for the electrodes preparation.

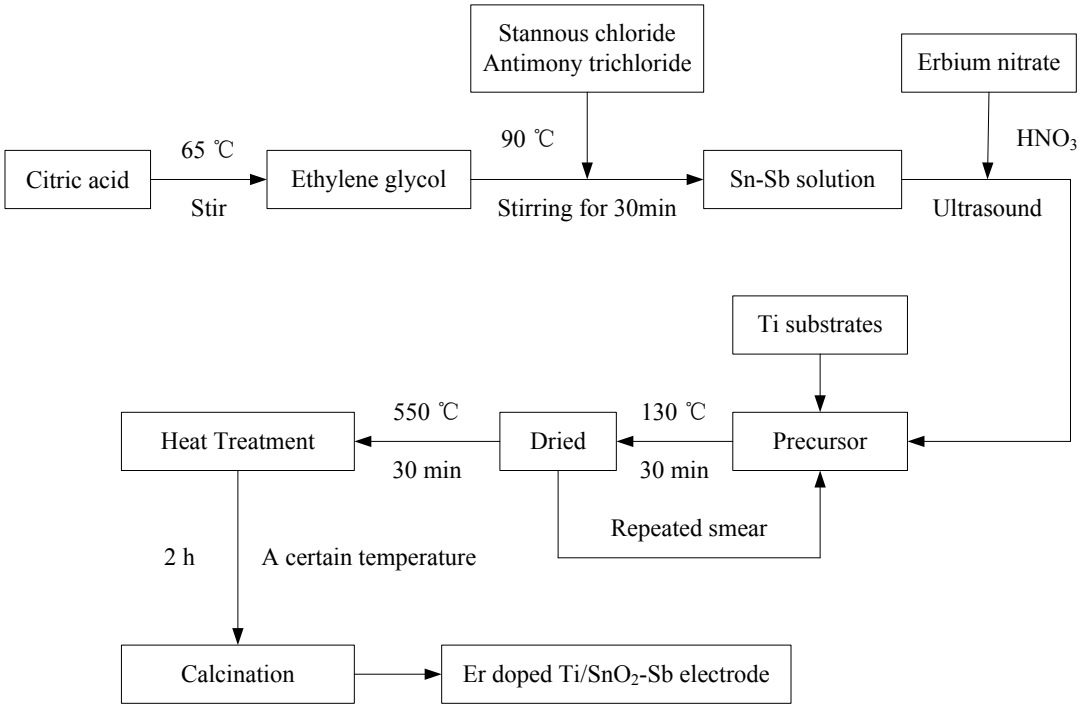

Fig. S10 Electrode preparation process chart with citric acid chelate precursor method.

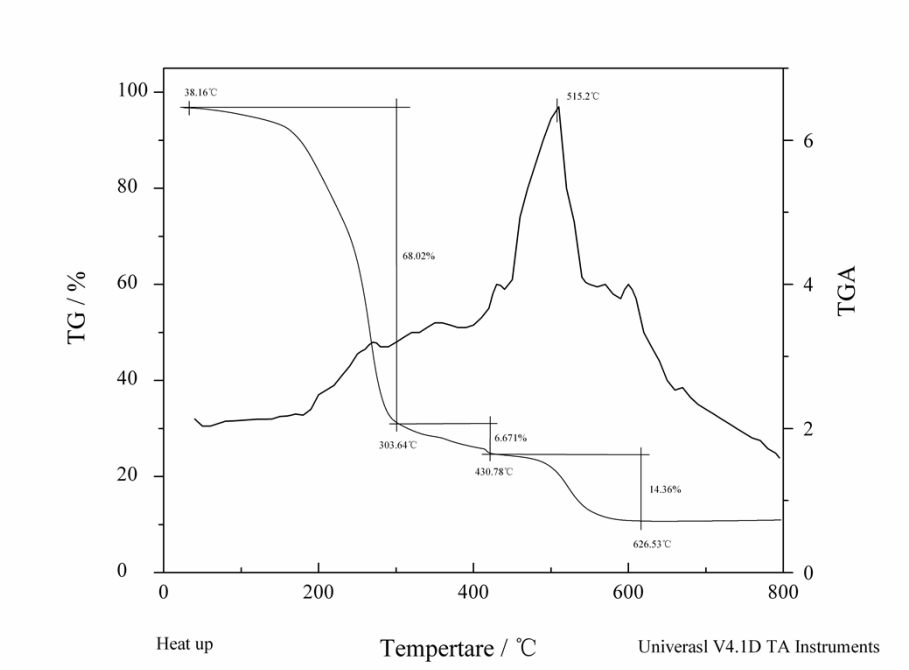

Fig. S11 TG-DTA spectrogram of the xerogel sample without Er doping.

References

1 D. He, S.I. Mho, Electroanal. Chem., 2004, 568, 19-27.

2 D. X., Tang, L. X., Wang, The Chinese J. Rare Earths., 1992, 10, 66-71.

3 O. Acarbas, E. Suvaci, A. Dog, Ceram. Int., 2007, 33, 537-542.

4 S. K. Pillai, L. M. Sikhwivhilua, T. K. Hillie, Mater. Chem. Phys., 2010, 120, 619-624.

5 Y. Q. Shao，D. Tang, Heat Treat. Mental., 2006, 31, 16-18.

6 E. Kokufuta, T. Shibasaki, I. Nakamura, J. Chem. Soc., 1985, 2, 100-102.

7 B. Sun, M. Sato, A. Harano, J. Electrostat., 1998, 43, 115-126.

8 K. P. Reis, V. K. Joshi, M. E. Thompson, J. Catal., 1996, 161, 62-67.